Am J Physiol Cell Physiol 303: C204–C212, 2012.
First published May 9, 2012; doi:10.1152/ajpcell.00059.2012.

Lipopolysaccharide-sensitive H^+ current in dendritic cells

Kalina Szteyn, Wenting Yang, Evi Schmid, Florian Lang, and Ekaterina Shumilina

Department of Physiology, University of Tübingen, Tübingen, Germany

Submitted 28 February 2012; accepted in final form 2 May 2012

Szteyn K, Yang W, Schmid E, Lang F, Shumilina E. Lipopolysaccharide-sensitive H^+ current in dendritic cells. *Am J Physiol Cell Physiol* 303: C204–C212, 2012. First published May 9, 2012; doi:10.1152/ajpcell.00059.2012.—Dendritic cells (DCs) are the most potent antigen-presenting cells equipped to transport antigens from the periphery to lymphoid tissues and to present them to T cells. Ligation of Toll-like receptor 4 (TLR4), expressed on the DC surface, by lipopolysaccharides (LPS), elements of the Gram-negative bacteria outer wall, induces DC maturation. Initial steps of maturation include stimulation of antigen endocytosis and enhanced reactive oxygen species (ROS) production with eventual downregulation of endocytic capacity in fully matured DCs. ROS production depends on NADPH oxidase (NOX2), the activity of which requires continuous pH and charge compensation. The present study demonstrates, for the first time, the functional expression of voltage-gated proton (Hv1) channels in mouse bone marrow-derived DCs. In whole cell patch-clamp experiments, we recorded Zn^{2+} (50 μM)-sensitive outwardly rectifying currents activated upon depolarization, which were highly selective for H^+, with the reversal potential shift of 38 mV per pH unit. The threshold voltage of activation ($V_{threshold}$) was dependent on the pH gradient and was close to the empirically predicted $V_{threshold}$ for the Hv1 currents. LPS (1 μg/ml) had bimodal effects on Hv1 channels: acute LPS treatment increased Hv1 channel activity, whereas 24 h of LPS incubation significantly inhibited Hv1 currents and decreased ROS production. Activation of H^+ currents by acute application of LPS was abolished by PKC inhibitor GFX (10 nM). According to electron current measurements, acute LPS application was associated with increased NOX2 activity.

voltage-gated proton channel; NADPH oxidase; NOX2; protein kinase C

ALMOST FOUR DECADES AGO, dendritic cells (DCs) were recognized as a novel cell population localized in mouse lymphoid organs (50). The present knowledge allows DCs to be placed in the center of immunological responses as they are crucial for eliciting immunity and maintaining tolerance. DCs develop from the hematopoietic stem cells in the bone marrow and share common myeloid progenitors with monocytes, megakaryocytes, erythrocytes, macrophages, and granulocytes (25). Committed DC precursors leave bone marrow and, through blood, are distributed to peripheral tissues where they differentiate into several subsets characterized by specific surface protein markers (27). DCs are the most potent antigen presenting cells of the immune system. Immature DCs are positioned at the periphery, where they sample the environment and recognize "danger" signals (1). After detection of an antigen, DCs start a complex process of maturation and migrate to the T cell zones of draining lymph nodes (1). Mature DCs present antigens on their major histocompatibility complexes (MHC) during formation of the so-called immunological synapse with naïve antigen-specific T cells (18). This tight apposition lasts 6–18 h (12) and involves membrane proteins at the interface between T cells and antigen presenting DCs as well as soluble chemical signals like cytokines (20).

One of the hallmarks of DCs is their high endocytic activity at the immature state, which is lost with maturation (15). However, recently it has been demonstrated that, even though mature DCs completely shut down macropinocytosis, they are still able to accomplish receptor-mediated endocytosis (40). One of the endocytic mechanisms widely used by DCs is phagocytosis, a complex process that starts with assembling of NADPH oxidase NOX2 multicomplex at the phagocytic site (48). In DCs, NOX2 regulates antigen processing, shifting the balance from total destruction, typical for neutrophils and macrophages, towards preservation of peptide fragments that subsequently can be associated with MHCII proteins and presented to naïve T cells (47). Two mechanisms attributed to NOX2-dependent reduction of phagosomal proteolysis in DCs have been proposed: *1*) by keeping phagosomal pH in the alkaline range 7.5–7.3 in the first 4 h of phagocytosis, due to constant low production of reactive oxygen species (ROS) and consumption of protons, as shown in the study of Amigorena group (29, 48) or *2*) by non-pH redox-mediated mechanism affecting the activity of local cysteine cathepsins, as shown by Rybicka et al. (45). $Gp91^{phox}$ subunit of NOX2 enzyme contains an electron transport chain that translocates electrons from the cytoplasmic NADPH to the extracellular or intraphagosomal O_2 that is reduced to superoxide anion ($O_2^{\cdot -}$), a precursor to various other ROS, such as H_2O_2 or HOCl (22), the production of which consumes large amounts of protons (45, 48). Without charge compensation mechanism, electrogenic NOX2 activity would generate +200 mV depolarization above the resting potential in 20 ms, which would cease its activity (10). In addition, accumulation of H^+ upon NADPH oxidation and constant NADPH regeneration would decrease cytoplasmic pH to the levels that diminish NOX2 performance (33). Therefore, charge compensation and prevention of low cytosolic pH are indispensable for sustained NOX2 activity.

Even though proton currents were detected already in 1991 (5), the *Hvcn1* gene coding for voltage-gated proton channels (Hv1) was identified in humans (42) and mice (46) as late as 2006. The voltage-gating domain of proton channels resembles that of other voltage-gated channels, although lacking S5-S6 pore-forming domains (7). The lack of a pore domain (42) and the perfect proton selectivity suggest that permeation in this channel occurs by a hydrogen-bonded chain mechanism including side chains of amino acids (9, 37). Recently aspartate 112 has been identified to form the selectivity filter of the human voltage-gated proton channel (37).

Proton channels are activated by depolarization with the activation becoming faster at more depolarized voltages (9), but what really distinguishes them from other channels is their pH-dependent gating. Decrease in intracellular (pH_i) or increase in extracellular (pH_o) pH causes a shift in the conductance-voltage relationship 40 mV/unit pH towards more neg-

Address for reprint requests and other correspondence: E. Shumilina, Physiologisches Institut der Universität Tübingen, Gmelinstr. 5, D-72076 Tübingen, Germany (e-mail: ekaterina.shumilina@uni-tuebingen.de).

ative voltages (8). The most effective inhibitor of the voltage-gated proton channels is Zn^{2+} (51). The action of Zn^{2+} slows the activation and shifts the conductance-voltage relationship towards more positive voltages (4). The potency of Zn^{2+} greatly decreases at low pH_o, suggesting competition between H^+ and Zn^{2+} for binding sites on the channel (4).

The primary functions of proton channels are acid extrusion and charge compensation during respiratory burst in phagocytic cells. Accordingly, NADPH oxidase activity is decreased by 75% in leukocytes from Hv1-deficient mice (43), a finding confirming previous reports that NADPH oxidase activity is associated with Hv1 and not with other Zn^{2+}-sensitive molecules (7).

ROS production is virtually absent in DC phagosomes from *gp91-phox*-deficient mice, indicating that NOX2 is responsible for ROS production during phagocytosis in DCs (48). Lipopolysaccharide (LPS) stimulation promotes ROS production in RAW264.7 cells, HEK293T cells overexpressing Toll-like receptor 4 (TLR4), and bone marrow-derived DCs (30, 38, 44).

In the present study we demonstrate by whole cell patch-clamp experiments the expression of functional Hv1 channels in DCs. Furthermore, we present evidence that acute stimulation of DCs with LPS causes a PKC inhibitor-sensitive increase in Hv1 channel activity. At the same time, activation of NOX2 by LPS was detected by appearance of electron currents, sensitive to the NOX2 inhibitor diphenylene iodonium (DPI). The stimulating effect of LPS on Hv1 channels was transient as at the advanced stage of LPS-induced maturation a reduction of proton currents was observed.

MATERIALS AND METHODS

Cell culture. Dendritic cells were isolated from the bone marrow of 7- to 12-wk-old mice of C57BL/6 or 129/SvJ background as previously described (31). Briefly, bone marrow cells were flushed out of the cavities of femur and tibia with PBS and washed twice with RPMI 1640 (PAA Laboratories). Cells were seeded with a density of 2×10^6 per 60-mm dish. Cells were cultured for 6 days in RPMI 1640, supplemented with 10% FCS, 1% penicillin-streptomycin, 1% glutamine, 1% nonessential amino acids (NEAA), 0.05% β-mercaptoethanol, and granulocyte-macrophage colony-stimulating factor (GM-CSF; 35 ng/ml, Immunotools). Cells were fed with fresh medium on the 3rd and the 6th day. Experiments were performed on DCs at *days 7* through *11*.

Patch clamp. Patch-clamp experiments were performed at room temperature in voltage-clamp, fast whole cell mode according to Hamill et al. (21). The cells were continuously superfused through a flow system inserted into a dish. The bath was grounded via a bridge filled with NaCl Ringer solution. Borosilicate glass pipettes (2–4 MΩ tip resistance, Harvard Apparatus) were prepared with the use of a microprocessor-driven puller (Zeitz) and were used with a MS314 electrical micromanipulator (MW, Märzhäuser, Wetzlar, Germany). The currents were recorded by an EPC-9 amplifier (HEKA, Lambrecht, Germany) using Pulse software (HEKA) and an ITC-16 Interference (Instrutech, Port Washington, NY). Currents were generated by 4-s square wave voltage pulses from −80 to + 80 mV in 20-mV steps delivered from a holding potential of −80 mV, in 40-s intervals between pulses. Tail currents were elicited by 2-s voltage pulses to potentials between −110 mV and +30 mV following a depolarizing prepulse to +80 mV for 2 s. The currents were recorded with an acquisition frequency of 10 kHz and 3 kHz low-pass filtered. Leak currents were subtracted. Leak outward currents were estimated from the linear fit and extrapolation of the inward currents at negative voltages (where the H^+ channels are inactive). The liquid junction potential ΔE between the CsCl pipette and the NaCl bath solutions was estimated as described earlier (2). Data were corrected for the estimated ΔE values.

Solutions. NaCl Ringer bath solution contained (in mM) 145 NaCl, 5 KCl, 2 $CaCl_2$, 2 $MgCl_2$, 10 HEPES (pH 7.4, NaOH). $TMASO_3$ bath solution contained (in mM): 80 $(CH_3)_2SO_3$, 100 MES (pH 6.0)/100 HEPES (pH 7.0)/100 Tricine (pH 8.0), 2 $MgCl_2$, 1 EGTA. To measure electron currents, the bath solution contained in (mM) 75 CsCl, 50 CsOH, 50 HEPES, 10 tetraethyl ammonium chloride (TEACl), 1 MgCl2, and 0.1% glucose (pH 7.1 CsOH).

Where indicated, bath solutions were supplemented with 1 μg/ml LPS (Enzo Life Sciences), GFX (10 nM, Calbiochem), Zn^{2+} (50 μM, Sigma-Aldrich), DPI (10 μM, Sigma-Aldrich).

The patch-clamp pipettes were filled with either $TMASO_3$ solution containing (in mM) 80 $(CH_3)_2SO_3$, 100 MES (pH 6.0)/100 HEPES (pH 7.0)/100 Tricine (pH 8.0), 2 $MgCl_2$, and 1 EGTA; or CsCl pipette solution containing (in mM) 145 CsCl, 10 HEPES, 2 $MgCl_2$, 2 Mg-ATP, and 1 EGTA; or pipette solution for electron currents containing (in mM) 75 CsCl, 50 CsOH, 50 HEPES, 10 TEACl, 1 $MgCl_2$, 1 MgATP, and 8 NADPH (pH 7.6).

RT-PCR. Total RNA was extracted from mouse DCs in TriFast (Peqlab, Erlangen, Germany) according to the manufacturer's instructions. After DNAse digestion, reverse transcription of total RNA was performed using random hexamers (Roche Diagnostics, Penzberg, Germany) and SuperScriptII reverse transcriptase (Roche Diagnostics, Penzberg, Germany). Polymerase chain reaction (PCR) amplification of the respective genes was set up in a total volume of 20 μl using 40 ng of cDNA, 500 nM forward and reverse primer and 2× GoTaq qPCR Master Mix SYBR Green (Promega, Madison, WI) according to the manufacturer's protocol. Cycling conditions were as follows: initial denaturation at 95°C for 2 min, followed by 40 cycles of 95°C for 15 s, 55°C for 15 s and 68°C for 20 s. For the amplification, the following primers were used: Hvcn1 forward: 5′-TGCAAAGGAGTGCTGCAAACTA-3′, reverse: 5′-TCGAGTAGACGCTCCGCAAT-3′; NOX2 forward: 5′-ACTTCTTGGGTCAGCACTGG-3′, reverse: 5′-ATTCCTGTCCAGTTGTCTTCG-3′, Tbp forward: 5′-CAAGCTGGAGGTGATCATCG-3′, reverse: 5′-TCCACAGTGCTCTTGAATTCG-3′; GAPDH forward: 5′-TGTGTCCGTCGTGGATCTGA-3′, reverse: 5′-CCTGCTTCACCACCTTCTTGA-3′.

Specificity of the PCR product was confirmed by analysis of melting curve. Real-time PCR amplifications were performed on a CFX96 Real Time System (Bio-Rad). All experiments were done in duplicate. Amplification of the housekeeping genes *Tbp* (TATA-binding protein) or *GAPDH* was performed to standardize the amount of sample RNA. Relative quantification of gene expression was achieved with the ΔΔCt method (where Ct is threshold cycle) as described previously (39). In addition, PCR products were analyzed by agarose gel electrophoresis.

Western blot analysis. Cell lysates were separated by 10% SDS-PAGE and blotted on nitrocellulose membranes. The blots were blocked with 10% nonfat milk in triethanolamine-buffered saline (TBS) and 0.1% Tween 20. The blots were then probed overnight with one of the following antibodies: rabbit polyclonal Hv1 (1:200, 36 kDa, Alomone Labs), rabbit monoclonal NOX2 (1:1,000, 60 kDa, Epitomics), or rabbit monoclonal GAPDH (1:1,000, 37 kDa, Cell Signaling). All antibodies were diluted in TBS with 5% BSA and 0.1% Tween 20. The blots were then washed three times for 10 min/wash, probed with respective secondary antibodies (anti-rabbit, Cell Signaling) diluted 1:3,000 for 1 h at room temperature, and washed three times for 10 min/wash. Antibody binding was detected with the Western blotting detection reagents (Amersham ECL Western Blotting Detection Reagents, GE Healthcare). Densitometer scans of the blots were performed using Quantity One (Bio-Rad, Munich, Germany).

ROS production. ROS production in DCs was determined with use of 2′,7′-dichlorodihydrofluorescein diacetate (DCFDA, Sigma-Aldrich). Cells were collected and washed once with RPMI and resuspended in fresh medium at 1×10^6/ml density. DCs were stained with DC marker CD11c antibody (1:1,000 dilution, BD Biosciences) and

incubated for 1 h at 37°C. After 30 min of incubation with CD11c, DCFDA was added at the final concentration of 10 μM and the cells were incubated for another 30 min. Cells were washed twice with ice-cold PBS and resuspended in FACS buffer (PBS supplemented with 0.1% FCS), and the fluorescence was analyzed by flow cytometry. The CD11c intensity was measured at FL4, and DCFDA intensity was detected at FL1. Only cells positive for both markers were analyzed.

Statistics. Data are provided as means ± SE where *n* represents the number of independent experiments. All data were tested for significance using Student's unpaired or paired two-tailed *t*-test or two-tailed Welch-corrected unpaired *t*-test or ANOVA. The significance level was established at $P < 0.05$.

RESULTS

To assess whether mouse bone marrow-derived DCs express functional H^+ channels, patch-clamp whole cell experiments were performed with TMA^+-based pipette and bath solutions containing 100 mM buffer. Depolarizing pulses lasting 4 s between −80 and + 80 mV were applied from the holding potential of −80 mV in 20-mV steps at 40-s intervals. Figure 1 shows typical slowly activating outward currents and the mean current-voltage (*I–V*) relationships obtained at the end of 4-s pulses measured with pH_i of 6.0 (Fig. 1, *A* and *C*) and pH_i of 7.0 (Fig. 1*B*) and pH_o of 6.0, 7.0, and 8.0. The current amplitude increased with increasing pH gradient between pH_o and pH_i (ΔpH). The threshold voltage for the current activation shifted in general 40 mV per unit pH, towards more negative potentials, and was close to the threshold voltage predicted by the formula $V_{treshold} = 20 - 40 \times \Delta pH$ with $\Delta pH = pH_o - pH_i$. The currents were sensitive to 50 μM Zn^{2+}, a known inhibitor of H^+ channels (Fig. 1*C*).

The corresponding conductance-voltage curves are shown in Fig. 2. The chord conductance reached a limiting maximum when ΔpH was ≥1. The activation threshold $V_{threshold}$ was similar at the same ΔpH when measured with pH_i 6.0 and pH_i 7.0. Figure 2C shows the analysis of time-dependent activation

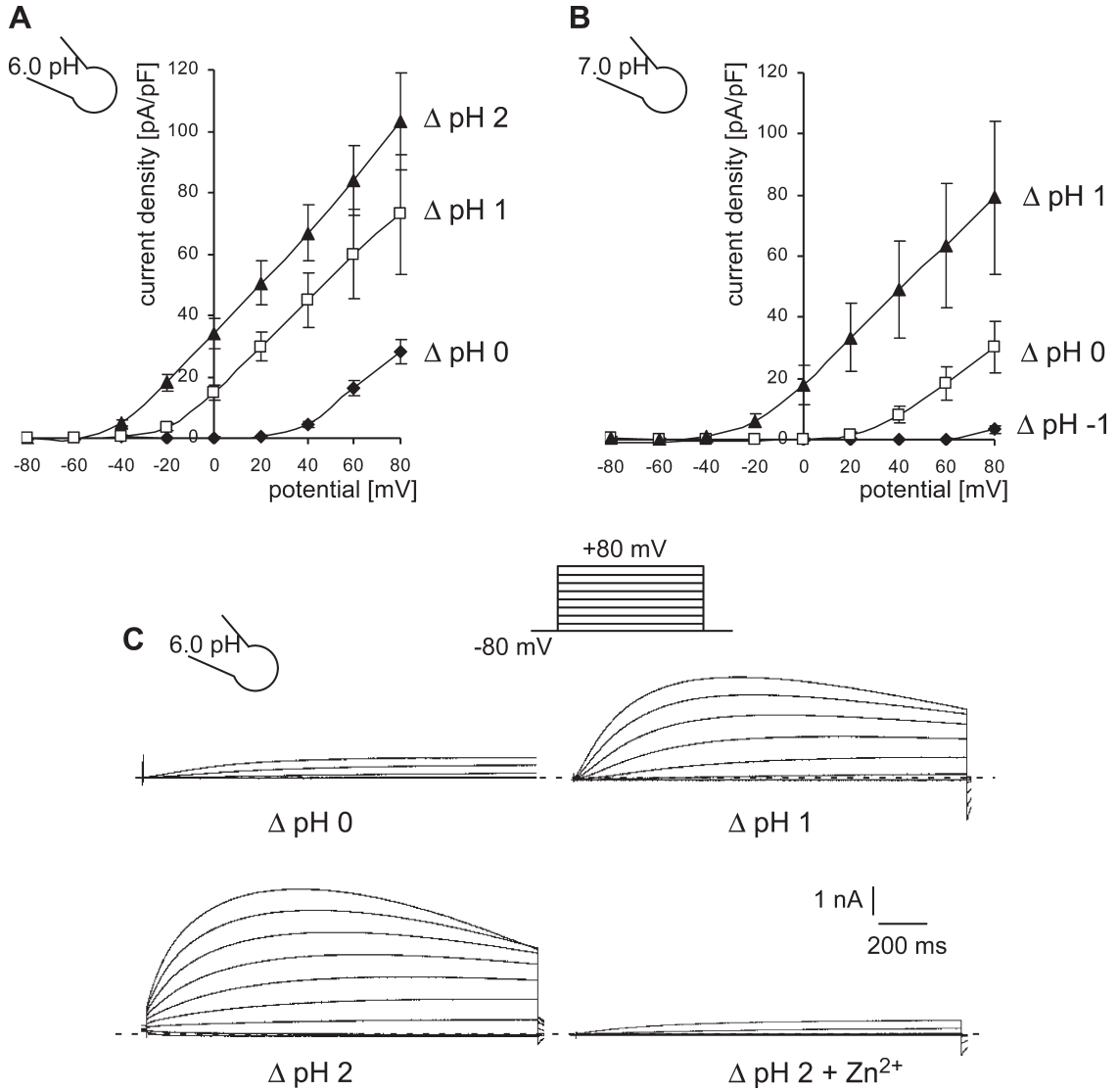

Fig. 1. Mean current-voltage (*I–V*) curves (± SE, n = 7–28) from mouse dendritic cells (DCs) recorded at intracellular pH (pH_i) 6.0 (*A*) or pH_i 7.0 (*B*) in the pipette solution and various bath extracellular pH (pH_o) values (6.0, 7.0, 8.0) and original current tracings obtained at pipette pH_i 6.0 and bath pH_o 6.0, 7.0, and 8.0 and finally after application of Zn^2 (50 μM) to the bath solution (*C*). The voltage protocol is shown (not to scale), whereby cells were held at −80 mV and voltage steps were applied in 20-mV increments for 4 s from −80 mV to +80 mV at 40-s intervals. Zero current is indicated by a dashed line.

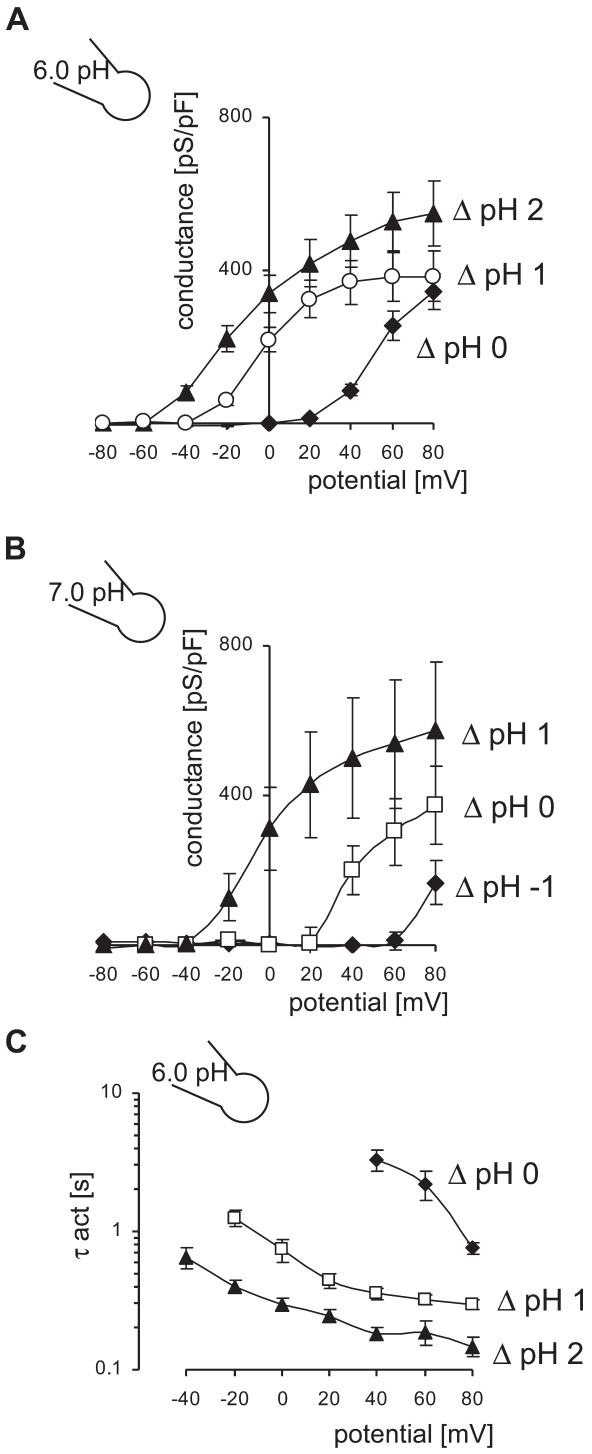

Fig. 2. *A* and *B*: mean conductance-voltage (g–V) relations (± SE, n = 7–28) at pipette pH_i 6.0 (*A*) and pH_i 7.0 (*B*) and various bath pH_o (6.0, 7.0, 8.0) values as calculated from the data in Fig. 1, *A* and *B*, respectively, assuming reversal potential at E_H. *C*: mean time constant of activation (τ_{act} ± SE, n = 12–24) determined by fitting monoexponential growth functions to the current tracings recorded at pH_i 6.0 and pH_o 6.0, 7.0, 8.0 upon cell depolarization to potentials between −40 mV and +80 mV as a function of membrane potential.

of the H^+ currents in DCs. The mean activation time constant (τ_{act}) was calculated from the fitting of the current tracings measured at pH_i of 6.0 and pH_o of 6.0, 7.0, and 8.0 with a monoexponential growth function. The τ_{act} decreased (i.e., the faster activation) with stronger depolarization and increasing ΔpH (Fig. 2C).

To estimate the reversal potential (V_{rev}), tail currents were measured at pH_i 6.0 and various pH_o (6.0, 7.0, 7.5, and 8.0) (Fig. 3, *A* and *B*). Plotting V_{rev} against ΔpH and fitting the data by linear regression yielded a slope of −38 mV/ΔpH, indicating a 38-mV shift in V_{rev} per pH unit, which differs from the theoretical equilibrium potential calculated with the use of the Nernst equation of −58 mV. However, the measured channels were highly selective for H^+ with a permeability ratio P_H/P_{TMA} of 1.94×10^6 at ΔpH = 2.0, calculated with the Goldman-Hodgkin-Katz equation.

The time constant of deactivation (τ_{tail}) obtained by fitting the tail currents with a monoexponential decay function showed an exponential dependence on the voltages and changed e-fold every 22.5 ± 0.6 mV (Fig. 3*C*). Finally, Hv1 mRNA is expressed in bone marrow-derived DCs, as demonstrated by RT-PCR analysis (Fig. 3*D*). Together, these data allow the conclusion that DCs express functional H^+ channels.

H^+ currents in DCs were extremely sensitive to the maturation stimulus, such as LPS, a ligand of TLR4. When the full-blown maturation was induced by 24 h of treatment with LPS (1 μg/ml), the amplitude of H^+ currents in DCs was strongly decreased (Fig. 4, *A* and *B*). At the same time, LPS-matured DCs significantly decreased the production of ROS as measured by FACS with the ROS-sensitive dye DCFDA (10 μM) (Fig. 4*C*). The decline of the H^+ currents was paralleled with a decrease in the transcript abundance of Hv1, as assessed by quantitative RT-PCR (Fig. 4*D*). However, no change in Hv1 protein level was observed (Fig. 4*E*). Expression of NOX2 was not significantly different in LPS-matured DCs when compared with immature cells (Fig. 4, *D* and *E*).

However, an early triggering of TLR4 with LPS is known to transiently increase the phagocytic abilities of DCs (53). Consistently, we analyzed the H^+ currents upon acute application of LPS under more "physiological" conditions: with CsCl in the pipette and NaCl in the bath and ΔpH = 0.2. Under these conditions, the threshold voltage of activation $V_{treshold}$ was about +20 mV in the absence of LPS, which was slightly more positive than the $V_{treshold}$ predicted by the formula (+12 mV) (Fig. 5*A*). Addition of LPS (1 μg/ml) to the bath solution caused a significant increase of the outward Zn^{2+} (50 μM)-inhibited conductance and a shift of the $V_{treshold}$ towards more negative potentials (Fig. 5, *A* and *B*). Stimulation of H^+ currents by LPS required functional PKC, since inhibiting PKC with GFX (10 nM) abolished this effect (Fig. 5*C*). At the same time, NOX2 activation could be observed by the appearance of LPS-induced electron currents. To measure electron currents, the experimental conditions were designed to minimize the currents through other channels and transporters (49). The measurements were performed in the presence of 300 μM niflumic acid, to avoid the contribution of Cl^- currents. Furthermore, the "reversed" pH gradient (pH_i of 7.6 and pH_o of 7.1) and the 0-mV holding potential allowed to exclude H^+ currents. The measured currents were indeed not modified by addition of 50 μM Zn^{2+} to the bath solutions (Fig. 5*D*). The mean electron current density at 0 mV was 0.16 ± 0.03 pA/pF (n = 9), measured with the pipette solution containing NADPH (8 mM) (Fig. 5D). These currents were inhibited by the NOX2

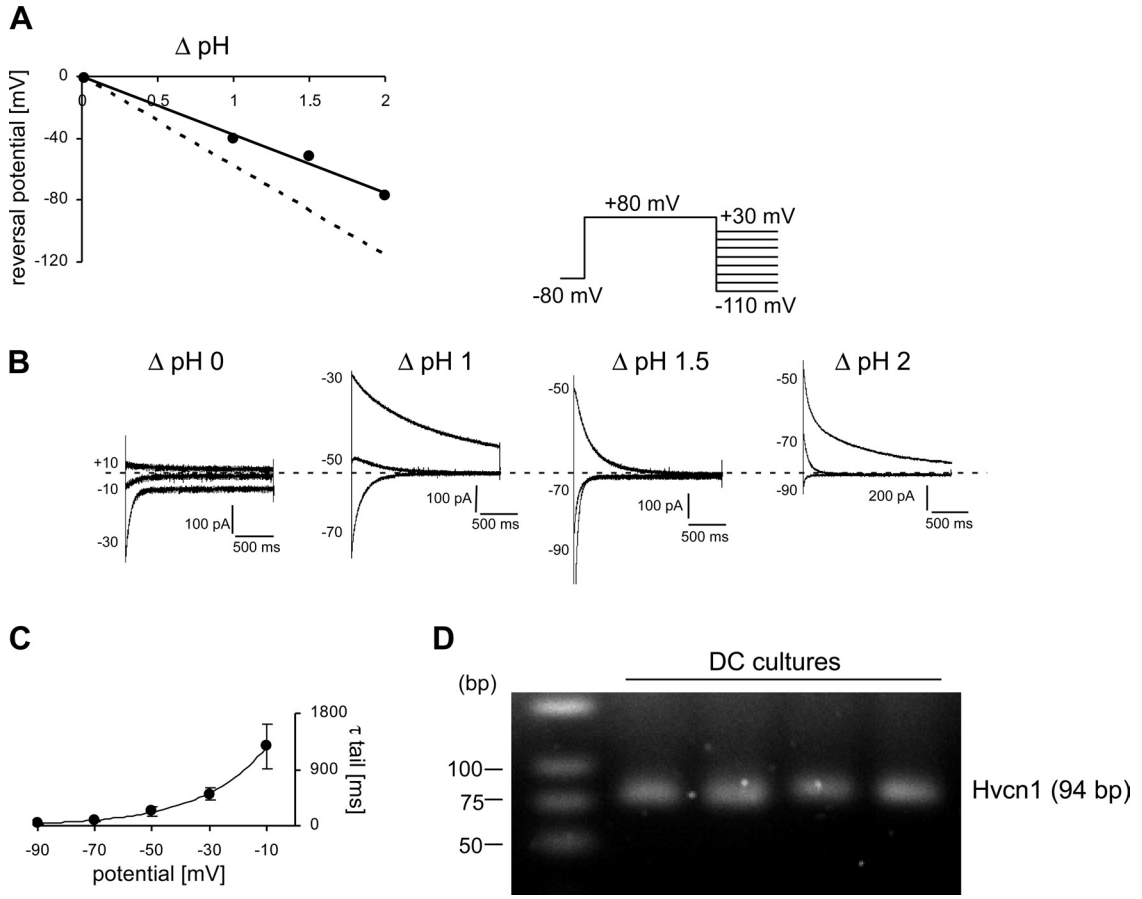

Fig. 3. *A* and *B*: mean values of the reversal potential (± SE, $n = 4–6$) as a function of ΔpH determined by tail currents at pH_i 6.0 in the pipette solution and bath pH_o values of 6.0, 7.0, 7.5, 8.0. Data were fitted by linear regression with a slope of −38 mV/pH unit. The equilibrium Nernst potential for H^+ with a slope of −58 mV/pH unit is shown by the dashed line. To record tail currents, depolarizing prepulse was given to +80 mV for 2 s, after which the membrane potential was clamped from −110 mV to +30 mV. Original tail currents at ΔpH 0, 1, 1.5, and 2.0 (*B*). *C*: mean time constant of deactivation (τ_{tail} ± SE, $n = 6–9$) determined by fitting the tail currents measured at −10 mV to −90 mV by a monoexponential decay function. *D*: agarose gel with PCR products specific for Hvcn1 amplified from cDNA isolated from 4 different cultures of mouse DCs. Specificity of the PCR product was confirmed by analysis of melting curves, and the right size of the products was confirmed by the agarose gel.

blocker DPI (10 μM, Fig. 5*D*). Immature human DCs under phorbol-12-myristate-13-acetate (PMA) stimulation generate superoxide anions ($O_2^{\cdot -}$) in approximate amounts of 2 nM $O_2^{\cdot -}$ per minute per 10^6 cells (52). When translated into electron currents, NADPH oxidase should transport $\sim 2 \times 10^7$ electrons per second per cell, giving the rough estimate of the expected inward currents with the amplitude of 2–4 pA (49), which is in agreement with our measurements (Fig. 5*D*).

DISCUSSION

The present study reports the functional expression of H^+ channels in mouse DCs by direct patch-clamp studies. Measured currents exhibited typical properties of H^+ currents observed in other cells (6), such as strongly outwardly rectifying *I–V* relationship, high selectivity for H^+, dependence of the threshold voltage of activation on the pH gradient, slow time-dependent activation kinetics upon depolarization, and sensitivity to Zn^{2+}. The reversal potential of −38 mV at ΔpH = 1 obtained in this study differs from the theoretical equilibrium potential calculated with the use of the Nernst equation of −58 mV. However, the cells having large H^+ currents could accumulate protons on the extracellular side of the membrane before all protons can be buffered. The local extracellular pH could become more acidic than the overall pH of the bath solution. This would lower the local pH gradient so that the reversal potential does not follow the predicted values. The selectivity of the H^+ channel measured in the present study was extremely high, the channel was more than 10^6 times more permeable for H^+ than for TMA^+.

The H^+ current amplitude in mouse DCs reached 56 pA/pF (when analyzed at +60 mV at pH_i of 6.0 and pH_o 7.5, which is about 150 mV positive to the reversal potential). The amplitude was similar to the H^+ current amplitude in mouse neutrophils [~50 pA/pF at pH_i 7.0 (14)] but higher than in mouse macrophages [30 pA/pF at pH_i 6.0 (23)] and mast cells [9.6 pA/pF at pH_i 5.5 (26)]. Among all cells in which the expression of H^+ channels has been established directly by patch-clamp studies, only human B lymphocytes [94.7 pA/pF at pH_i 6.0 (11)], human eosinophils [~200 pA/pF at pH_i 6.0 (17)], and human basophils [~100 pA/pF at pH_i 5.5 (36)] have shown higher H^+ current density than the current density observed here in DCs.

The main established function of Hv1 channels is to mediate H^+ efflux upon respiratory burst during phagocytosis (7). In

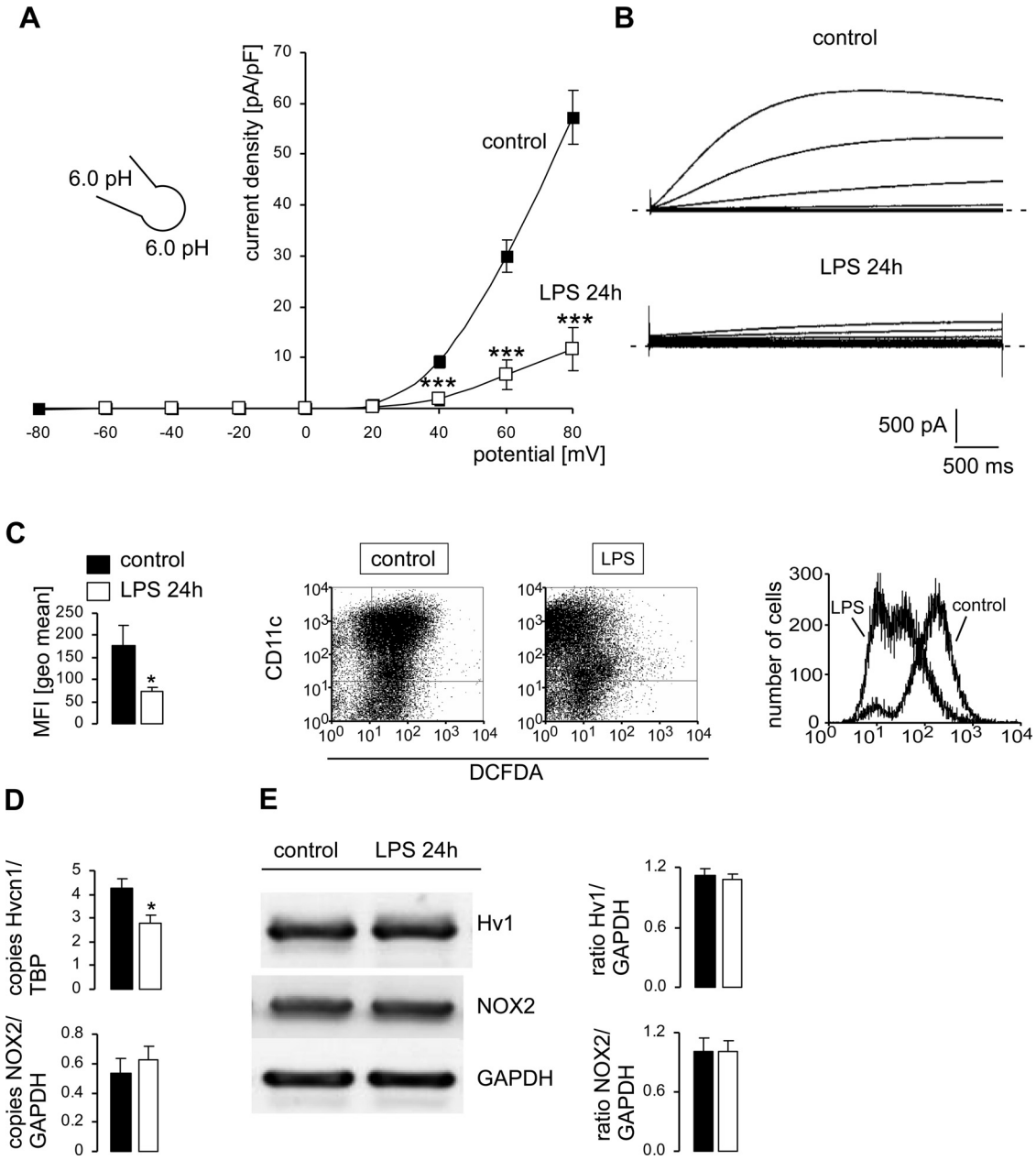

Fig. 4. *A* and *B*: mean *I–V* curves (± SE, *A*) and original current tracings (*B*) of immature (control, $n = 20$) and LPS (1 μg/ml, 24 h, $n = 12$)-matured DCs measured at pH 6.0 in pipette and bath solution. ***$P < 0.001$, two-tailed unpaired *t*-test. Zero current is indicated by dashed line. *C*: reactive oxygen species (ROS) production, analyzed as mean fluorescent intensity (MFI ± SE, $n = 17$, *left*) in immature (control) and LPS (1 μg/ml, 24 h)-matured DCs measured from ROS-dependent 2′,7′-dichlorodihydrofluorescein diacetate (DCFDA) fluorescence by FACS. *$P < 0.05$, Welch-corrected two-tailed unpaired *t*-test. Original dot plots of $CD11c^+$ DCFDA (*middle*) and histograms of DCFDA fluorescence on $CD11c^+$ cells (*right*) in a representative experiment. *D*: Hvcn1 (*top*) and NADPH oxidase NOX2 (*bottom*) mRNA levels (± SE, $n = 3–7$) determined after isolation from immature (control) and LPS (1 μg/ml, 24 h)-matured DCs and assessed by real-time PCR using TATA-binding protein (TBP) or GAPDH mRNA as a reference gene. *$P < 0.05$, two-tailed unpaired *t*-test. *E*: representative Western blot showing voltage-gated proton channel Hv1, NOX2, and GAPDH as a loading control (*left*) and mean Hv1/GAPDH and NOX2/GAPDH protein ratio (± SE, $n = 7$, *right*) in immature (control) and LPS (1 μg/ml, 24 h)-matured DCs.

granulocytes and macrophages, phagocytosis starts with the so-called respiratory burst characterized by an extremely high activity of NADPH oxidase (NOX2) and $O_2^{\cdot -}$ production (7). Activation of even a fraction of available NADPH oxidase may result in a depolarization sufficient to activate H^+ channels in phagocytes (34, 41). Hv1 activity supports the function of NOX2 by charge compensation and by H^+ extrusion (7). Accordingly, $O_2^{\cdot -}$ production within the first few minutes after PMA (phorbol myristate acetate)-induced activation of NOX2 is decreased by 75% in granulocytes from $Hv1^{-/-}$ mice (43).

While in neutrophils and macrophages phagocytosis is followed by complete degradation of captured dangerous particles (47), in DCs, phagocytosis progresses more gently, allowing to preserve peptide fragments for the presentation on MHCII (1). The reduced proteolytic efficiency in DCs strongly depends on NOX2 activity (45, 48), although DCs express only 5% of

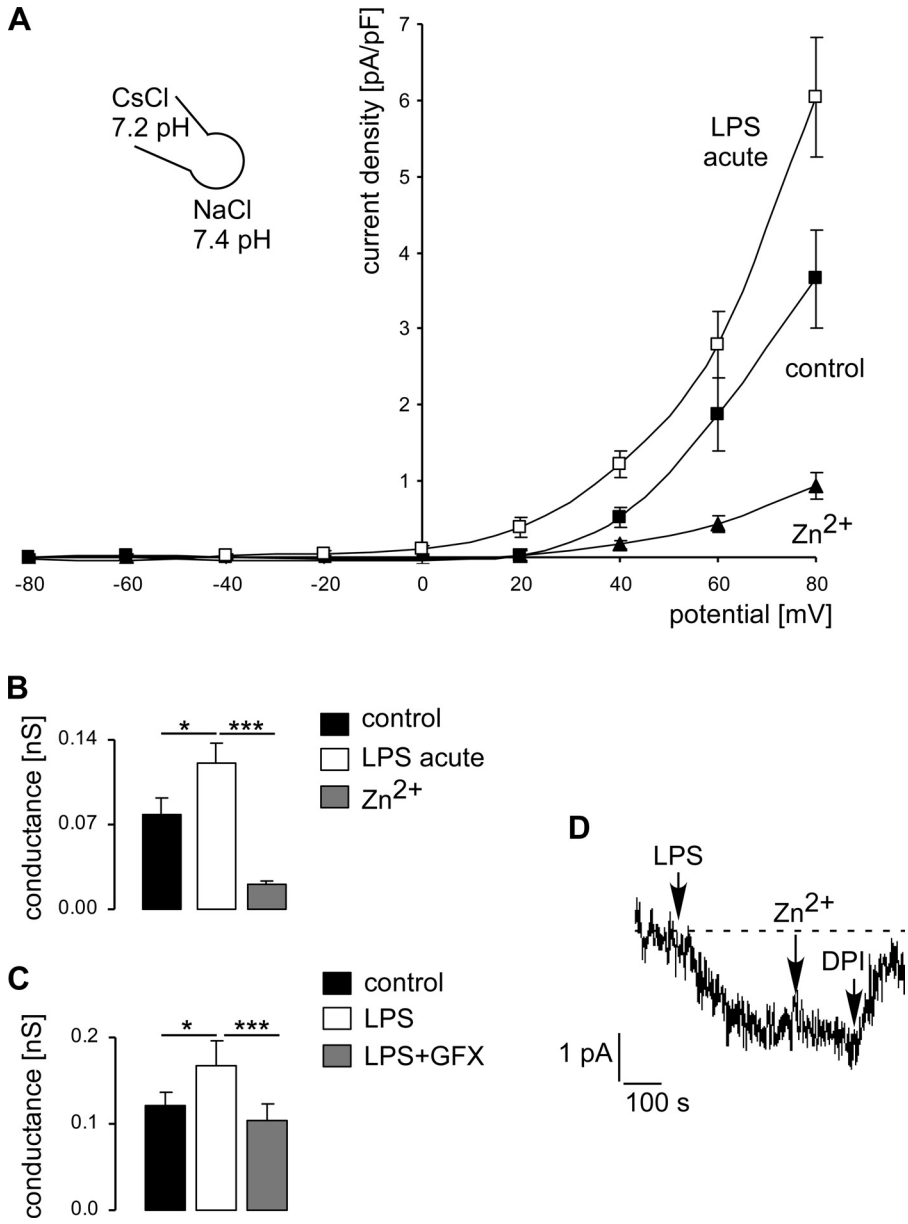

Fig. 5. *A*: mean *I–V* curves (± SE, $n = 19$) of immature DCs measured with CsCl pipette (pH 7.2) and NaCl bath (pH 7.4) solutions before (control) and after application of LPS (1 μg/ml) first in the absence (LPS acute) and then in the presence of Zn^{2+} (50 μM). *B*: mean current conductance (± SE, $n = 19$) calculated from individual *I–V* curves as in *A* by linear regression of the current between +40 and +80 mV. $*P < 0.05$ and $***P < 0.001$, ANOVA. *C*: mean conductance (± SE, $n = 11$) calculated from individual *I–V* curves by linear regression of the current between +40 and +80 mV obtained in paired experiments before (control) and after application of LPS (1 μg/ml) in the absence (LPS) and in the presence (LPS + GFX) of PKC inhibitor GFX (10 nM). $*P < 0.05$ and $***P < 0.001$, repeated-measures ANOVA. *D*: original whole cell inward currents generated by NADPH oxidase upon application of LPS (1 μg/ml) in DCs. The measurements were performed in the presence of 300 μM niflumic acid and with the "reversed" pH gradient (pH_i of 7.6 and pH_o of 7.1). Where indicated, Zn^{2+} (50 μM, to exclude the contribution of H^+ channels) and the NADPH oxidase inhibitor diphenylene iodonium (DPI; 20 μM) were added to the bath solution. CsCl-based bath and CsCl-based pipette solutions, containing 8 mM NADPH, were used, and the holding potential was 0 mV. Zero current is indicated by dashed line.

NOX2 in comparison to neutrophils (13). However, unlike the pattern observed in neutrophils and macrophages, NOX2 in DCs is associated for an extended period with the phagosomes and the NOX2 activity is sustained beyond 1 h after internalization of the particles (29, 45, 48). NOX2-mediated ROS production in DCs has been proposed to result in proton consumption in the phagosome lumen, causing phagosomal alkalinization (48). However, in a recent study, in which real-time fluorimetry of DC phagosomes has been performed, DCs have been able to fully acidify their phagosomes to a pH below 5.0 within 30 min and the mechanism of NOX2-dependent control of phagosomal proteolysis has been shown to be pH-independent involving redox modulation of local cysteine cathepsines (45). In any case, NOX2 activity requires charge compensation and proton translocation into the phagosomes. The Hv1 channel is perfectly suited to perform both functions simultaneously. As shown recently, phagosomal NOX2 activity is indeed moderately attenuated in Hv1-deficient mouse DCs (45).

In the present study, the classical agent inducing DC maturation, LPS, a ligand of TLR4, stimulated H^+ currents when applied acutely but reduced Hv1 channel mRNA abundance and H^+ currents after 24 h of incubation. The Hv1 protein abundance was, however, not changed by 24 h of incubation with LPS. Stimulation of H^+ currents by acute LPS treatment was accompanied by a fast activation of NOX2 and generation of NOX2 electron currents. The activation of H^+ channels by acute LPS application seems to result from the LPS-dependent stimulation of PKC, since the stimulating effect of LPS was abolished by inhibition of PKC with GFX. PKC is known to be involved in signaling downstream from TLRs (28). On the other hand, PKC phosphorylates Hv1 channel on the threonine 29 (35), resulting in enhanced gating mode of Hv1 (32) with increased maximal H^+ conductance and a 40-mV shift in the

threshold voltage of activation towards more negative potentials (32, 35), which is close to the observed alterations of H^+ currents upon acute stimulation of DCs with LPS in the present study.

Activation of Hv1 channel by LPS could support NOX2 activity and promote antigen uptake and ROS production in DCs. Upon LPS stimulation, a transient increase in the ability of DCs to uptake soluble antigens and immune phagocytable complex antigens was observed (3, 16, 53). ROS production is enhanced by LPS in RAW264.7 cells, HEK293T cells overexpressing TLR4, and bone marrow-derived DCs (30, 38, 44). Moreover, direct interaction between TLR4 and NADPH oxidase has been shown in HEK293T cells (38). It is tempting to speculate that PKC dependent Hv1 channel regulation might underlie the previously reported decrease in LPS-induced phagocytosis in murine microglia upon inhibition of PKCδ (24), the isoform that phosphorylates Hv1 (35).

Inhibition of H^+ currents after 24 h stimulation of DCs with LPS may reflect the loss of endocytic capacity in mature DCs (54). It has been shown that the early increase in endocytic capacity upon LPS stimulation in DCs peaks 2 h after ligation of the TLR4 receptor (53) and then the ability for endocytosis is gradually lost becoming strongly reduced after 18 h stimulation with LPS (19). Moreover, as observed in the present study, ROS production was also diminished in LPS-matured DCs.

In conclusion, our study demonstrates the functional expression of LPS-regulated Hv1 channels in mouse DCs, regulated by LPS in a bimodal way with acute PKC-dependent stimulation followed by a strong reduction of H^+ currents in fully matured DCs treated with LPS for 24 h.

DISCLOSURES

No conflicts of interest, financial or otherwise, are declared by the author(s).

AUTHOR CONTRIBUTIONS

K. Szteyn, W. Yang, and E. Schmid performed experiments; K. Szteyn and E. Shumilina analyzed data; K. Szteyn and E. Shumilina interpreted the results of the experiments; K. Szteyn and E. Shumilina prepared the figures; K. Szteyn and E. Shumilina drafted the manuscript; K. Szteyn, F. Lang, and E. Shumilina edited and revised the manuscript; E. Shumilina conception and design of the research; E. Shumilina approved the final version of the manuscript.

REFERENCES

1. **Banchereau J, Briere F, Caux C, Davoust J, Lebecque S, Liu YJ, Pulendran B, Palucka K.** Immunobiology of dendritic cells. *Annu Rev Immunol* 18: 767–811, 2000.
2. **Barry PH, Lynch JW.** Liquid junction potentials and small cell effects in patch-clamp analysis. *J Membr Biol* 121: 101–117, 1991.
3. **Blander JM, Medzhitov R.** Regulation of phagosome maturation by signals from toll-like receptors. *Science* 304: 1014–1018, 2004.
4. **Cherny VV, DeCoursey TE.** pH-dependent inhibition of voltage-gated H^+ currents in rat alveolar epithelial cells by Zn^{2+} and other divalent cations. *J Gen Physiol* 114: 819–838, 1999.
5. **DeCoursey TE.** Hydrogen ion currents in rat alveolar epithelial cells. *Biophys J* 60: 1243–1253, 1991.
6. **DeCoursey TE.** Voltage-gated proton channels. *Cell Mol Life Sci* 65: 2554–2573, 2008.
7. **DeCoursey TE.** Voltage-gated proton channels find their dream job managing the respiratory burst in phagocytes. *Physiology (Bethesda)* 25: 27–40, 2010.
8. **DeCoursey TE, Cherny VV.** Deuterium isotope effects on permeation and gating of proton channels in rat alveolar epithelium. *J Gen Physiol* 109: 415–434, 1997.
9. **DeCoursey TE, Cherny VV.** Voltage-activated hydrogen ion currents. *J Membr Biol* 141: 203–223, 1994.
10. **DeCoursey TE, Morgan D, Cherny VV.** The voltage dependence of NADPH oxidase reveals why phagocytes need proton channels. *Nature* 422: 531–534, 2003.
11. **Demaurex N, El Chemaly A.** Physiological roles of voltage-gated proton channels in leukocytes. *J Physiol* 588: 4659–4665, 2010.
12. **Dustin ML, Chakraborty AK, Shaw AS.** Understanding the structure and function of the immunological synapse. *Cold Spring Harb Perspect Biol* 2: a002311, 2010.
13. **Elsen S, Doussiere J, Villiers CL, Faure M, Berthier R, Papaioannou A, Grandvaux N, Marche PN, Vignais PV.** Cryptic O_2^--generating NADPH oxidase in dendritic cells. *J Cell Sci* 117: 2215–2226, 2004.
14. **Essin K, Salanova B, Kettritz R, Sausbier M, Luft FC, Kraus D, Bohn E, Autenrieth IB, Peschel A, Ruth P, Gollasch M.** Large-conductance calcium-activated potassium channel activity is absent in human and mouse neutrophils and is not required for innate immunity. *Am J Physiol Cell Physiol* 293: C45–C54, 2007.
15. **Garrett WS, Chen LM, Kroschewski R, Ebersold M, Turley S, Trombetta S, Galan JE, Mellman I.** Developmental control of endocytosis in dendritic cells by Cdc42. *Cell* 102: 325–334, 2000.
16. **Gil-Torregrosa BC, Lennon-Dumenil AM, Kessler B, Guermonprez P, Ploegh HL, Fruci D, van Endert P, Amigorena S.** Control of cross-presentation during dendritic cell maturation. *Eur J Immunol* 34: 398–407, 2004.
17. **Gordienko DV, Tare M, Parveen S, Fenech CJ, Robinson C, Bolton TB.** Voltage-activated proton current in eosinophils from human blood. *J Physiol* 496: 299–316, 1996.
18. **Grakoui A, Bromley SK, Sumen C, Davis MM, Shaw AS, Allen PM, Dustin ML.** The immunological synapse: a molecular machine controlling T cell activation. *Science* 285: 221–227, 1999.
19. **Granucci F, Ferrero E, Foti M, Aggujaro D, Vettoretto K, Ricciardi-Castagnoli P.** Early events in dendritic cell maturation induced by LPS. *Microbes Infect* 1: 1079–1084, 1999.
20. **Griffiths GM, Tsun A, Stinchcombe JC.** The immunological synapse: a focal point for endocytosis and exocytosis. *J Cell Biol* 189: 399–406, 2010.
21. **Hamill OP, Marty A, Neher E, Sakmann B, Sigworth FJ.** Improved patch-clamp techniques for high-resolution current recording from cells and cell-free membrane patches. *Pflügers Arch* 391: 85–100, 1981.
22. **Henderson LM, Chappell JB, Jones OT.** The superoxide-generating NADPH oxidase of human neutrophils is electrogenic and associated with an H^+ channel. *Biochem J* 246: 325–329, 1987.
23. **Kapus A, Romanek R, Qu AY, Rotstein OD, Grinstein S.** A pH-sensitive and voltage-dependent proton conductance in the plasma membrane of macrophages. *J Gen Physiol* 102: 729–760, 1993.
24. **Kim DC, Kim SH, Jeong MW, Baek NI, Kim KT.** Effect of rottlerin, a PKC-delta inhibitor, on TLR-4-dependent activation of murine microglia. *Biochem Biophys Res Commun* 337: 110–115, 2005.
25. **Kondo M, Scherer DC, King AG, Manz MG, Weissman IL.** Lymphocyte development from hematopoietic stem cells. *Curr Opin Genet Dev* 11: 520–526, 2001.
26. **Kuno M, Kawawaki J, Nakamura F.** A highly temperature-sensitive proton current in mouse bone marrow-derived mast cells. *J Gen Physiol* 109: 731–740, 1997.
27. **Liu K, Nussenzweig MC.** Origin and development of dendritic cells. *Immunol Rev* 234: 45–54, 2010.
28. **Loegering DJ, Lennartz MR.** Protein kinase C and toll-like receptor signaling. *Enzyme Res* 2011: 537821, 2011.
29. **Mantegazza AR, Savina A, Vermeulen M, Perez L, Geffner J, Hermine O, Rosenzweig SD, Faure F, Amigorena S.** NADPH oxidase controls phagosomal pH and antigen cross-presentation in human dendritic cells. *Blood* 112: 4712–4722, 2008.
30. **Matsuzawa A, Saegusa K, Noguchi T, Sadamitsu C, Nishitoh H, Nagai S, Koyasu S, Matsumoto K, Takeda K, Ichijo H.** ROS-dependent activation of the TRAF6-ASK1-p38 pathway is selectively required for TLR4-mediated innate immunity. *Nat Immunol* 6: 587–592, 2005.
31. **Matzner N, Zemtsova IM, Nguyen TX, Duszenko M, Shumilina E, Lang F.** Ion channels modulating mouse dendritic cell functions. *J Immunol* 181: 6803–6809, 2008.
32. **Morgan D, Cherny VV, Finnegan A, Bollinger J, Gelb MH, DeCoursey TE.** Sustained activation of proton channels and NADPH oxidase in human eosinophils and murine granulocytes requires PKC but not cPLA2 alpha activity. *J Physiol* 579: 327–344, 2007.

33. **Morgan D, Cherny VV, Murphy R, Katz BZ, DeCoursey TE.** The pH dependence of NADPH oxidase in human eosinophils. *J Physiol* 569: 419–431, 2005.
34. **Murphy R, DeCoursey TE.** Charge compensation during the phagocyte respiratory burst. *Biochim Biophys Acta* 1757: 996–1011, 2006.
35. **Musset B, Capasso M, Cherny VV, Morgan D, Bhamrah M, Dyer MJ, DeCoursey TE.** Identification of Thr29 as a critical phosphorylation site that activates the human proton channel *Hvcn1* in leukocytes. *J Biol Chem* 285: 5117–5121, 2010.
36. **Musset B, Morgan D, Cherny VV, MacGlashan DW Jr, Thomas LL, Rios E, DeCoursey TE.** A pH-stabilizing role of voltage-gated proton channels in IgE-mediated activation of human basophils. *Proc Natl Acad Sci USA* 105: 11020–11025, 2008.
37. **Musset B, Smith SM, Rajan S, Morgan D, Cherny VV, Decoursey TE.** Aspartate 112 is the selectivity filter of the human voltage-gated proton channel. *Nature* 480: 273–277, 2011.
38. **Park HS, Jung HY, Park EY, Kim J, Lee WJ, Bae YS.** Cutting edge: direct interaction of TLR4 with NAD(P)H oxidase 4 isozyme is essential for lipopolysaccharide-induced production of reactive oxygen species and activation of NF-kappa B. *J Immunol* 173: 3589–3593, 2004.
39. **Pfaffl MW.** A new mathematical model for relative quantification in real-time RT-PCR. *Nucleic Acids Res* 29: e45, 2001.
40. **Platt CD, Ma JK, Chalouni C, Ebersold M, Bou-Reslan H, Carano RA, Mellman I, Delamarre L.** Mature dendritic cells use endocytic receptors to capture and present antigens. *Proc Natl Acad Sci USA* 107: 4287–4292, 2010.
41. **Rada BK, Geiszt M, Kaldi K, Timar C, Ligeti E.** Dual role of phagocytic NADPH oxidase in bacterial killing. *Blood* 104: 2947–2953, 2004.
42. **Ramsey IS, Moran MM, Chong JA, Clapham DE.** A voltage-gated proton-selective channel lacking the pore domain. *Nature* 440: 1213–1216, 2006.
43. **Ramsey IS, Ruchti E, Kaczmarek JS, Clapham DE.** Hv1 proton channels are required for high-level NADPH oxidase-dependent superoxide production during the phagocyte respiratory burst. *Proc Natl Acad Sci USA* 106: 7642–7647, 2009.
44. **Rotte A, Pasham V, Eichenmuller M, Mahmud H, Xuan NT, Shumilina E, Gotz F, Lang F.** Effect of bacterial lipopolysaccharide on Na^+/H^+ exchanger activity in dendritic cells. *Cell Physiol Biochem* 26: 553–562, 2010.
45. **Rybicka JM, Balce DR, Chaudhuri S, Allan ER, Yates RM.** Phagosomal proteolysis in dendritic cells is modulated by NADPH oxidase in a pH-independent manner. *EMBO J* 31: 932–944, 2011.
46. **Sasaki M, Takagi M, Okamura Y.** A voltage sensor-domain protein is a voltage-gated proton channel. *Science* 312: 589–592, 2006.
47. **Savina A, Amigorena S.** Phagocytosis and antigen presentation in dendritic cells. *Immunol Rev* 219: 143–156, 2007.
48. **Savina A, Jancic C, Hugues S, Guermonprez P, Vargas P, Moura IC, Lennon-Dumenil AM, Seabra MC, Raposo G, Amigorena S.** NOX2 controls phagosomal pH to regulate antigen processing during crosspresentation by dendritic cells. *Cell* 126: 205–218, 2006.
49. **Schrenzel J, Serrander L, Banfi B, Nusse O, Fouyouzi R, Lew DP, Demaurex N, Krause KH.** Electron currents generated by the human phagocyte NADPH oxidase. *Nature* 392: 734–737, 1998.
50. **Steinman RM, Cohn ZA.** Identification of a novel cell type in peripheral lymphoid organs of mice. I. Morphology, quantitation, tissue distribution. *J Exp Med* 137: 1142–1162, 1973.
51. **Thomas RC, Meech RW.** Hydrogen ion currents and intracellular pH in depolarized voltage-clamped snail neurones. *Nature* 299: 826–828, 1982.
52. **Vulcano M, Dusi S, Lissandrini D, Badolato R, Mazzi P, Riboldi E, Borroni E, Calleri A, Donini M, Plebani A, Notarangelo L, Musso T, Sozzani S.** Toll receptor-mediated regulation of NADPH oxidase in human dendritic cells. *J Immunol* 173: 5749–5756, 2004.
53. **West MA, Wallin RP, Matthews SP, Svensson HG, Zaru R, Ljunggren HG, Prescott AR, Watts C.** Enhanced dendritic cell antigen capture via toll-like receptor-induced actin remodeling. *Science* 305: 1153–1157, 2004.
54. **Zanoni I, Granucci F.** Regulation of antigen uptake, migration, and lifespan of dendritic cell by Toll-like receptors. *J Mol Med* 88: 873–880, 2010.